© 2020 by the Arizona Board of Regents on behalf of the University of Arizona

## RADIOCARBON RESERVOIR AGES IN THE HOLOCENE DEAD SEA

Nurit Weber<sup>1,2</sup> • Boaz Lazar<sup>1</sup> • Ofra Stern<sup>1,2</sup> • George Burr<sup>3,4</sup> • Ittai Gavrieli<sup>2</sup> • Mark Roberts<sup>5</sup> • Mark D Kurz<sup>5</sup> • Yoseph Yechieli<sup>2,6</sup> • Mordechai Stein<sup>1,2</sup>

<sup>1</sup>The Fredy and Nadine Herrmann Institute of Earth Sciences, The Hebrew University of Jerusalem, The Edmund Safra Campus, Givat-Ram, Jerusalem 9190401, Israel

**ABSTRACT.** The sources and fate of radiocarbon (<sup>14</sup>C) in the Dead Sea hypersaline solution are evaluated with <sup>14</sup>C measurements in organic debris and primary aragonite collected from exposures of the Holocene Ze'elim Formation. The reservoir age (RA) is defined as the difference between the radiocarbon age of the aragonite at time of its precipitation (representing lake's dissolved inorganic carbon [DIC]) and the age of contemporaneous organic debris (representing atmospheric radiocarbon). Evaluation of the data for the past 6000 yr from Dead Sea sediments reveal that the lake's RA decreased from 2890 yr at 6 cal kyr BP to 2300 yr at present. The RA lies at ~2400 yr during the past 3000 yr, when the lake was characterized by continuous deposition of primary aragonite, which implies a continuous supply of freshwater-bicarbonate into the lake. This process reflects the overall stability of the hydrological-climate conditions in the lake's watershed during the late Holocene where bicarbonate originated from dissolution of the surface cover in the watershed that was transported to the Dead Sea by the freshwater runoff. An excellent correlation (R<sup>2</sup>=0.98) exists between aragonite ages and contemporaneous organic debris, allowing the estimation of ages of various primary deposits where organic debris are not available.

**KEYWORDS:** aragonite, Dead Sea, Holocene, radiocarbon, reservoir ages.

### INTRODUCTION

Radiocarbon (<sup>14</sup>C) dating of primary carbonates (i.e. aragonite, calcite) requires an estimation of the <sup>14</sup>C "reservoir age" (RA), a property that describes the age equivalent of the radiocarbon content of the dissolved inorganic carbon (DIC) in the precipitating solution at the time of mineral deposition.

The <sup>14</sup>C RA, t<sub>RA</sub>, at the time of carbonate precipitation is defined here by the following equation:

$$t_{RA} = -\frac{1}{\lambda} \cdot \ln \frac{F_{RA}}{F_{atm,t}} \tag{1}$$

Where:  $\lambda$  is the Libby decay constant of  $^{14}$ C (1/8033 yr $^{-1}$ , Stuiver and Polach 1977);  $F_{RA}$  is the fraction of radiocarbon (F is expressed in fraction of modern carbon units [fMC]) in the carbonate mineral (considered to be equal to the fraction of radiocarbon in water's DIC) at the time of its precipitation, t; and  $F_{atm,t}$  is the fraction of radiocarbon in atmosphere's  $CO_2$  at the same time, t. The time t is the calendar age of organic debris collected from the same stratigraphic horizon as the carbonate mineral, which can be determined also by any independent chronological method, such as U-Th dating, e.g. Schramm et al. 2000.

Typically, the DI $^{14}$ C/DIC ratio of the precipitating solution is lower than the  $^{14}$ CO $_2$ /CO $_2$  ratio of the contemporaneous atmosphere (F<1) due to mixing with different proportions of older (or even "dead") carbon. Minerals of Ca-carbonates, typically aragonite, that were formed in the late Quaternary lakes that filled the tectonic depression of the Dead Sea Basin (e.g. the last

<sup>&</sup>lt;sup>2</sup>Geological Survey of Israel, 32 Yesha'ayahu Leibowitz St., Jerusalem 9692100, Israel

<sup>&</sup>lt;sup>3</sup>NSF-Arizona AMS Laboratory, University of Arizona, Tucson AZ 85721-0081, USA

<sup>&</sup>lt;sup>4</sup>Department of Geosciences, National Taiwan University, Taipei, Taiwan

<sup>&</sup>lt;sup>5</sup>NOSAMS, Woods Hole Oceanographic Institution, Woods Hole, MA 02543, USA

<sup>&</sup>lt;sup>6</sup>Department of Hydrology and Microbiology, Zuckerberg Center, Ben-Gurion University of the Negev, Sede Boker 8499000, Israel

<sup>\*</sup>Corresponding author. Email: nurit.weber@mail.huji.ac.il.

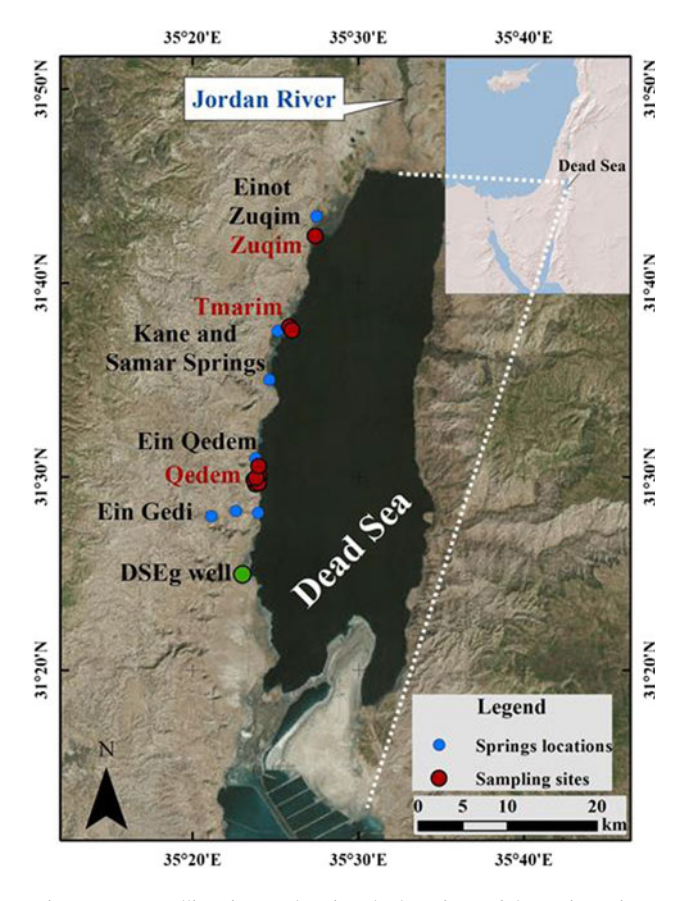


Figure 1 Satellite picture showing the locations of the main springs (solid blue circles, black fonts), the sampling sites (solid red circles, red fonts) and the location of Ein Gedi (DSEg) well (solid green circle, black font) on western shore of the Dead Sea. The inset shows the location of the Dead Sea within the eastern Mediterranean. (Please see electronic version for color figures.)

glacial Lake Lisan and the Holocene Dead Sea, see review in Stein 2001) incorporated in their lattice <sup>14</sup>C from the lake's DIC (e.g., the pioneering work of W.S. Broecker in: Begin et al. 1985; and later works by Stein et al. 2000; Bookman et al. 2007; Prasad et al. 2009). The lake received its dissolved <sup>14</sup>C from various water types, hence, radiocarbon content in the CaCO<sub>3</sub> minerals that precipitated in the lake can be used as a monitor of its hydrological history, provided the age of the mineral is estimated independently (e.g., by U-Th dating, Haase-Schramm et al. 2004). The lakes that occupied the Dead Sea basin were fed by different fresh-to-hypersaline water sources characterized by distinct apparent <sup>14</sup>C ages, which reflected their hydrological histories (Belmaker et al. 2007; Stein et al. 2004, 2013). The <sup>14</sup>C content in these sources have rather wide range, from ~1 fMC (atmospheric <sup>14</sup>C values) for runoff waters, almost equilibrated with the atmospheric CO<sub>2</sub> (Belmaker et al. 2007) to ~0.04–0.1 fMC in the Ein Qedem saline springs (Weber et al. 2018) that currently discharge to the Dead Sea (Figure 1 for location). The origin of the Ein Qedem springs, based on its chemical composition and radiocarbon content, was attributed to the epilimnetic brine of

the last glacial Lake Lisan that infiltrated the marginal aquifers at ~25 cal kyr BP, when the lake reached its highest stand (Weber et al. 2018). Stein et al. 2004 calculated RA of the Holocene Dead Sea using pairs of aragonite and organic debris from the same stratigraphic horizons in a sediment core drilled at Ein Gedi spa (DSEg, see Figure 1 for location). The calculated RA values range from ~6000 to 2200 yr, the high RA value was related to enhanced contribution of an old Ca-chloride brine that discharged from saline springs during low stands of the lake, and the lower RA values were attributed to addition of freshwaters that equilibrated with the atmosphere (Stein et al. 2004).

Here, we expand the study on the behavior of radiocarbon (and the RA) in the Holocene Dead Sea and its use as a paleohydrological monitor of the Dead Sea water-system (e.g., the contribution of freshwater to the lake during the Holocene). The work is based on high resolution <sup>14</sup>C analyses of organic debris and co-existing primary aragonite from the exposed sections of the Ze'elim Formation that was deposited at the Dead Sea during the Holocene (Ken-Tor et al. 2001; Migowski et al. 2006; Stein, 2014) at the Qedem shore (Figure 1). The sedimentary section at the Qedem shore comprises sequences of aragonite and gypsum that appear as layers and crusts (Table 1, Figure 2) that were deposited in the Holocene Dead Sea during the past ~7000 years (part of the Ze'elim Fm.). The Qedem shore is also pitted with "gypsum structures" (Figure 2a, Table 2). We measured the radiocarbon contents in carbonate material and organic debris from the Qedem "gypsum structures" and similar structures that are exposed along the retreating western shores of the Dead Sea. The radiocarbon dating of the "gypsum structures" is a part of the ongoing investigation on their formation mechanism.

### SAMPLES AND METHODS

# **Materials and Analytical Methods**

Samples of aragonite, gypsum and organic debris were collected from exposures of the Holocene Ze'elim Formation (Fm.) and from "gypsum structures" at the shores of the Ein Qedem saline springs and at the Tmarim and Zuqim shores (Figures 1 and 2). The samples are listed and described in Tables 1 and 2.

Aragonite samples were collected from five columnar sections of the Ze'elim Fm. (Figure 2c) at the Qedem shore (Figure 1). Two hundred milligrams of physically separated aragonite material were washed 3 times in distilled water to remove soluble salts. The samples were dried under 60°C and were transformed to a preparatory line for extraction of CO<sub>2</sub> in the radiocarbon facility at the University of Arizona. The samples were dissolved in H<sub>3</sub>PO<sub>4</sub> (70%) and the released CO<sub>2</sub> was collected and graphitized. Radiocarbon was measured at the Accelerator Mass Spectrometry (AMS) facility at the University of Arizona.

Bulk gypsum samples were collected from the "Gypsum cliff" and the "Gypsum structures" along the Qedem shore (five samples), the Tmarim shore (two samples) and the Zuqim shore (one sample) (Table 2, locations are marked in Figure 1 and Figure 2 a,b). The bulk rock "gypsum" samples contain variable amounts of carbonate material (calcite and aragonite) which was used for the radiocarbon analysis. The bulk rock gypsum was ground to powder and the relative amounts of the major mineral phases: gypsum, aragonite and calcite were determined by XRD. The carbonate content was also measured by a "Carbonate Bomb" (computerized and modified version of the "Karbonat-Bombe" of Müller and Gastner, 1971). Then, targeting to have 3 mg of C, bulk powder was weighted

Table 1  $\,^{14}\mathrm{C}$  ages measured on pairs of aragonite and organic debris from the Ze'elim Formation, Holocene Dead Sea. The pairs were sampled from same stratigraphic horizons along the EG core and from columnar sections on the Qedem shore.

				Organic debris						Aragonite		
			Measur 14C ag	ed ge		<sup>3</sup> Calibrate <sup>14</sup> C age	ed	Measu <sup>14</sup> C a	ired .ge			
Sample	Site	Elevation (m bmsl)	(yr BP)	±	δ <sup>13</sup> C(‰)	(cal yr BP)	±	(yr BP)	±	δ <sup>13</sup> C(‰)	RA(yr)	± <sup>4</sup>
<sup>1</sup> DS-EN-33	EG core	415.02	160	30		140	140	2380	70		2220	80
<sup>1</sup> DS-EN-5	EG core	415.22	800	30		720	45	2970	70		2170	80
<sup>1</sup> DS-EN-61	EG core	416.7	1560	30		1460	70	3860	70		2300	80
<sup>1</sup> DS-EN-13	EG core	420.7	3680	30		4030	115	6090	40		2410	50
<sup>1</sup> DS-EN-47	EG core	424.42	5280	40		6060	120	7920	70		2640	80
<sup>1</sup> DS-EN-92	EG core	429.01	6460	70		7380	120	9850	70		3390	100
<sup>1</sup> DS-EN-83	EG core	430.88	6730	40		7590	75	12700	1200		5970	1200
<sup>1</sup> DS-EN-94	EG core	433.4	8200	40		9150	125	11500	1200		3300	1200
$^{2}G-30$	Qedem-1	417.7	5580	50	-23.6	6370	75	8470	50	-2.1	2890	70
$^{2}$ G-95	Qedem-1	417.1	4150	40	-22.6	4690	140	7090	40	5.2	2940	60
$^{2}G-240$	Qedem-1	415.6	3510	40	-26.4	3790	95	5930	40	2.6	2420	60
$^{2}G-260$	Qedem-1	415.4	3560	40	-9.3	3850	125	5830	40	0.9	2270	60
$^{2}G-275$	Qedem-1	415.3	3460	90	-23.4	3730	235	5780	40	-3	2320	100
$^{2}G-355$	Qedem-1	414.5	2890	80	-9.4	3060	260	5720	40	3.8	2830	90
$^{2}G-555$	Qedem-1	412.5	1000	30	-26.8	890	90	3540	30	3.5	2540	40
$^{2}G-650$	Qedem-1	411.5	640	30	-24.7	610	60	2800	30	-0.9	2160	40
$^{2}$ G-814	Qedem-1	409.9	1980	80	-26.4	1930	190	4370	40	1.3	2390	90

$^{2}$ S-1-25	Oedem-2	418.5	2800	70	-22.3	2930	170	5490	40	1	2690	80
$^{2}S-1-115$	Qedem-2	417.6	2950	30	-9.8	3100	110	5800	50	2.8	2850	60
$^{2}S-2-30$	Qedem-3	418.4	2640	80	-23.2	2720	225	5500	40	2.2	2860	90
$^{2}$ S-2-100	Qedem-3	417.7	6360	40	-24.1	7300	120	9420	50	1.1	3060	60
$^{2}$ S-2-160	Qedem-3	417.1	6640	80	-23	7540	115	9480	80	-3.2	2840	110
$^{2}$ S-2-300	Qedem-3	415.7	6320	100	-9.4	7210	220	9320	50	4.3	3000	110
$^{2}$ S-2-450	Qedem-3	414.2	3720	40	-11.3	4080	145	5950	110	5.4	2230	120
$^{2}$ S-2-525	Qedem-3	413.5	2690	80	-9.5	2760	240	5340	40	0.9	2650	90
$^{2}N-1-210$	Qedem-4	415.2	2080	80	-9.4	2090	215	4460	40	-2.6	2380	90
$^{2}N-1-460$	Qedem-4	412.7	2240	90	-9.4	2240	245	4700	40	3.9	2460	100
$^{2}N-2-50$	Qedem-5	417.1	7330	80	-25.7	8170	170	9270	50	-1.6	1940	90
$^{2}N-2-90$	Qedem-5	416.7	3720	80	-10.5	4100	245	6760	50	4.1	3040	90
<sup>2</sup> N-2-410	Qedem-5	413.5	2200	30	-19.9	2230	95	4640	40	-0.2	2440	50

<sup>&</sup>lt;sup>1</sup>Data from Stein et al. (2004).

<sup>&</sup>lt;sup>2</sup>Qedem site radiocarbon was measured at the AMS facilities at the University of Arizona.

<sup>&</sup>lt;sup>3</sup>The calibrated age was calculated from the radiocarbon (Libby) age by OxCal software (Oxford University). The reported age is the mean of the obtained range and the error of the age is the range divide by 2.

<sup>&</sup>lt;sup>4</sup>The error on  $t_{RA}$  was calculated by the equation:  $\Delta t_{RA} = \sqrt{\Delta t_{real}^2 + \Delta t_{app}^2}$  where )  $\Delta t_{real}$  and  $\Delta t_{app}$  are the error values of the <sup>14</sup>C age of the of organic debris as measured by AMS and  $\Delta$  the <sup>14</sup>C age of the aragonite, respectively.



Figure 2 The main geological features in the study area: (a) large "gypsum structure", a concentric mound composed of gypsum and aragonite layers; (b) large bladed gypsum crystals with thin layers of aragonite; (c) outcrop of the Ze'elim Formation on the Ein Qedem shore showing layers of gypsum, aragonite and detritus material.

and reacted overnight with H<sub>3</sub>PO<sub>4</sub> that released the CO<sub>2</sub> gas directly into a gas accepting ion source connected to the continuous-flow AMS system at the National Ocean Sciences AMS (NOSAMS) facility, Woods Hole (Roberts et al. 2013). Note that the radiocarbon analyses on the extracted aragonite are less precise than the other radiocarbon analyses (Table 2). This is because they were determined on the NOSAMS gas ion source, which requires rather large carbon content, as compared to the Cs sputtered graphite targets (all other measurements). The gas ion source was utilized because it allowed rapid and inexpensive reconnaissance measurements on a large number of gypsum-carbonate mixtures. Due to the complexity of the existence of aragonite and calcite in these mixtures, these larger uncertainties do not compromise the conclusions (see below).

Organic debris were collected from the same stratigraphic units as the aragonite and gypsum samples. The organic matter comprises small pieces of wood, visible to the naked eye (several cm long), carefully removed by tweezers from the outcrop in the field. The source of these organic debris is from spring vegetation around the lake or vegetation residues that were transported by floodwater from the lake's watershed. The organic debris were prepared for graphitization. Radiocarbon analyses were conducted at the AMS facilities at the University of Arizona (22 samples), Australian Nuclear Science and Technology Organisation (ANSTO) (3 samples), NOSAMS (3 samples) and Poznan Radiocarbon Laboratory, Poland (2 samples). The radiocarbon measurement uncertainty in all laboratories was smaller than 100 years. All the radiocarbon data were corrected for fractionation using  $\delta^{13}$ C results obtained by the various laboratories.

Table 2 <sup>14</sup>C ages of aragonite "trapped" in gypsum layers and <sup>14</sup>C ages on organic matter from the same stratigraphic horizons in several Holocene exposures along the Dead Sea shore.

					Organic debris								
Sample		Elevation	%	Aragonite fraction in	Measured <sup>14</sup> C age		<sup>1</sup> Calibrated <sup>14</sup> C age		Measured <sup>14</sup> C age		<sup>2</sup> Corrected <sup>14</sup> C age		
ID	Site	(m bmsl)	CaCO <sub>3</sub>	CaCO <sub>3</sub>	(yr BP)	±	(cal yr BP)	±	(yr BP)	±	(yr BP)	RA(yr)	±
NW-26	Tmarim	420.8	17	1	1360 <sup>(P)</sup>	30	1260	70	4010	130	4010	2650	130
NW-27	Tmarim	419.7	1.2	1	640 <sup>(P)</sup>	30	610	55	3970	120	3970	3330	120
NW-29	Zuqim	424.1	33.5	0.95	140 <sup>(N)</sup>	20	140	140	3240	120	2790	2650	120
NW-31	Qedem-6	423	11.3	0.78	1130 <sup>(A)</sup>	30	1070	105	6450	130	4360	3230	130
NW-32	Qedem-6	421	11.8	0.8	2380 (A)	30	2500	155	7090	130	5230	2850	130
NW-34	Qedem-6	417.6	12.6	0.86	3640 <sup>(A)</sup>	50	3990	150	9070	160	7780	4140	170
NW-41	Qedem-7	407.2	4.9	0.5	2050 (N)	30	2020	90	9680	160	3900	1850	160
NW-46	Qedem-8	419.1	11.7	0.83	3910 <sup>(N)</sup>	30	4340	85	7050	140	5530	1620	140

Organic debris radiocarbon analyses were measured at ANSTO<sup>(A)</sup>, NOSAMS<sup>(N)</sup> and Poznan<sup>(P)</sup>.

<sup>&</sup>lt;sup>1</sup>The calibrated age was calculated by OxCal software (Oxford University). The reported age is the mean of the obtained range and the error of the age is the range divide by 2.

<sup>&</sup>lt;sup>2</sup>Corrected <sup>14</sup>C age of the aragonite was calculated from the aragonite fraction in sample's CaCO<sub>3</sub> according to Eq. 6 of Bookman et al. (2007).

#### RESULTS

Radiocarbon measurements on aragonite laminae, or aragonite material within the bulk rock gypsum samples from the "gypsum structures" and their associated organic debris samples (taken from the same unit in the structure) are listed in Tables 1 and 2. The bulk rock gypsum samples contain 1.2–33.5 wt% carbonate (Table 2). In addition, the XRD analyses of the bulk rock gypsum samples show that in 6 of 8 samples the carbonate phase comprises a mixture of aragonite and calcite. The aragonite is a primary carbonate phase in this depositional environment while the calcite is detrital, derived from very old carbonate rocks (e.g., Haliva-Cohen et al. 2012). Together, these mineral phases are considered as the "carbonate material" that was dissolved by the phosphoric acid. Hence, the measured radiocarbon age for primary aragonite was corrected assuming the calcite fraction contains only "dead carbon" meaning that its <sup>14</sup>C content is zero (e.g., Bookman et al. 2007).

The RA of the lake is calculated according to Eq. (1). Since there is virtually no biological production in the water column of hypersaline Dead Sea, we assume that the sediment contains only detrital organic debris. These organic debris provide the "real" age of the layers ( $t_{real}$  in the equations thereafter).  $t_{real}$  is then used to obtain the atmospheric <sup>14</sup>C content applying IntCal13 and to calculate radiocarbon content of the lake (the F of the aragonite at time  $t_{real}$ ). Both radiocarbon values (atmospheric and lake's radiocarbon contents) are used to calculate the RA ( $t_{RA}$  in Eq. 1) during the time of aragonite deposition. The calculated RA values lie between ~2200 yr for the young samples (~ few hundred <sup>14</sup>C years) and ~6000 yr for the (almost) oldest (6730 <sup>14</sup>C yr) sample.

### **DISCUSSION**

## **DIC and Radiocarbon Mass-Balance Calculations**

The effects of various water inputs to the Dead Sea (that dictate the limnological configuration of the lake) on the RA of the lake, is formulated in the following simple mass balance equations for DIC and DI<sup>14</sup>C.

The DIC mass-balance is:

$$\frac{dC_{DS}}{dt} = \frac{1}{V_{DS}(Z(t))} \cdot \left[ DIC_{fl} \cdot Q_{fl} + DIC_{sp} \cdot Q_{sp} + DIC_{ss} \cdot Q_{ss} + DIC_{Jo} \cdot Q_{Jo} \right] - \frac{1}{Z(t)} \cdot \left[ R_{CaCO_3} + E_{CO_2} \right]$$
(2)

Where  $C_{DS}$  is the concentration of inorganic carbon [mol·m<sup>-3</sup>] of the lake, t is time [yr]; DIC<sub>i</sub> is the DIC in source/sink i [mol·m<sup>-3</sup>], the subscripts fl, sp, ss and jo denote the different water sources influx: floods, springs (fresh or brackish), saline springs and Jordan River, respectively;  $Q_i$  is the flux of water source i [m<sup>3</sup>·yr<sup>-1</sup>];  $V_{DS}$  is the volume of the lake [m<sup>3</sup>] as a function of depth (the hypsometric curve), Z(t) [m] at any specific time, t;  $R_{CaCO_3}$  and  $E_{CO_2}$  are the CaCO<sub>3</sub> precipitation rate and the net CO<sub>2</sub> escape rate from the Dead Sea, respectively [mol·m<sup>-2</sup>·yr<sup>-1</sup>].  $E_{CO_2}$  is expressed by the equation:

$$E_{CO_2} = k_{PV\_DS} \cdot K'_{H_{DS}} \cdot \left( P_{CO_2DS} - 400 \right) \cdot 10^{-6} \tag{3}$$

Where  $k_{PV\_DS}$  is the operational piston velocity of  $CO_2$  in the Dead Sea  $[m \cdot yr^{-1}]$ ,  $K'_{H_{DS}}$  is the Henry constant for Dead Sea brine  $[mol \cdot m^{-3} \cdot atm^{-1}]$ ;  $P_{CO_2DS}$  is the partial pressure of  $CO_2$  in the

Dead Sea [µatm] and the numbers 400 and 10<sup>-6</sup> are the present day partial pressure of atmospheric CO<sub>2</sub> [µatm] and the unit conversion factor from µatm to atm, respectively. We examined the sensitivity of the model to modern P<sub>CO</sub>, atmospheric changes for the model that represents the past 40 years (increase by ~75 µatm at Mauna Loa observatory) and found that the model is not sensitive to these changes and therefore uses a fixed, one significant digit figure.

The radiocarbon mass balance equation has similar form to that of Eq. (2), but each member contains a product of a particular source/sink DIC and its radiocarbon fraction (of modern atmospheric CO<sub>2</sub>), F [fMC]:

$$\begin{split} \frac{d(C_{DS} \cdot F_{DS})}{dt} &= \frac{1}{V_{DS}(Z(t))} \cdot \left[ DIC_{fl} \cdot Q_{fl} \cdot F_{fl} + DIC_{sp} \cdot Q_{sp} \cdot F_{sp} + DIC_{ss} \cdot Q_{ss} \cdot F_{ss} + DIC_{Jo} \cdot Q_{Jo} \cdot F_{jo} \right] \\ &- \frac{1}{Z(t)} \cdot \left[ R_{CaCO_3} \cdot F_{DS} + k_{PV_{DS}} \cdot k_{H_{DS}} \left( P_{CO_2DS} \cdot F_{DS} - 400 \cdot F_{atm} \right) \cdot 10^{-6} \right] \end{split} \tag{4}$$

Where the subscripts for all variables are the same as for Eq. (2) and Eq. (3). Note that radiocarbon decay was not included in Eq. (4), since the radiocarbon fluxes associated with all sources/sinks are much larger than the 14C decay flux (rate). Using the multiplication rule we separate the Dead Sea radiocarbon time derivative,  $\frac{dF_{DS}}{dt}$ , from the left side of Eq. (4) ( $\frac{d(C_{DS} \cdot F_{DS})}{dt}$ ) as follows:

$$\frac{dF_{DS}}{dt} = \frac{\frac{d(C_{DS} \cdot F_{DS})}{dt} - \frac{dC_{DS}}{dt} \cdot F_{DS}(t)}{C_{DS}(t)}$$
(5)

The F of lake's epilimnion at the time of the aragonite deposition, F<sub>RA</sub>, is calculated from the RA and the F of atmospheric <sup>14</sup>C for that time according to IntCal13 (F<sub>atm,t</sub>, Reimer et al. 2013) by rewriting Eq. (1):

$$ln(F_{RA}) = ln(F_{atm,t}) - \lambda \cdot t_{RA}$$
(6)

The equations presented in this section were used for calculating all parameters present in the following sections.

### The Effect of Various Influxes and Lake's Level Changes on the RA of the Lake

Temporal variations in RA of Lake Lisan and the Dead Sea were attributed to hydrologiclimnologic conditions, particularly to the relative contributions of freshwater and Ca-chloride brine (Schramm et al. 2000; Stein et al. 2004, 2013; Belmaker et al. 2007). Being a terminal lake, the Dead Sea surface level is sensitive to changes in the regional hydrological regime (Bartov et al. 2002, 2003; Bookman et al. 2004; Migowski et al. 2006; Torfstein et al. 2013). During periods of low lake stands the enhanced discharge of the saline springs contributed waters with very low 14C to the lake, while during long periods of high stand, a layered limnologic configuration was developed and the <sup>14</sup>C in the "isolated" hypolimnion may have partially decayed (Stein et al. 2004). According to the carbon mass balance models (Eqs. 2, 4) the variation in the RA of the lake depends directly on the product of water influx and the DIC concentration in this flux (the DIC "load"). This means that two environmental factors determine the RA in the lake: (1) The hydrological conditions that dictate the amount of

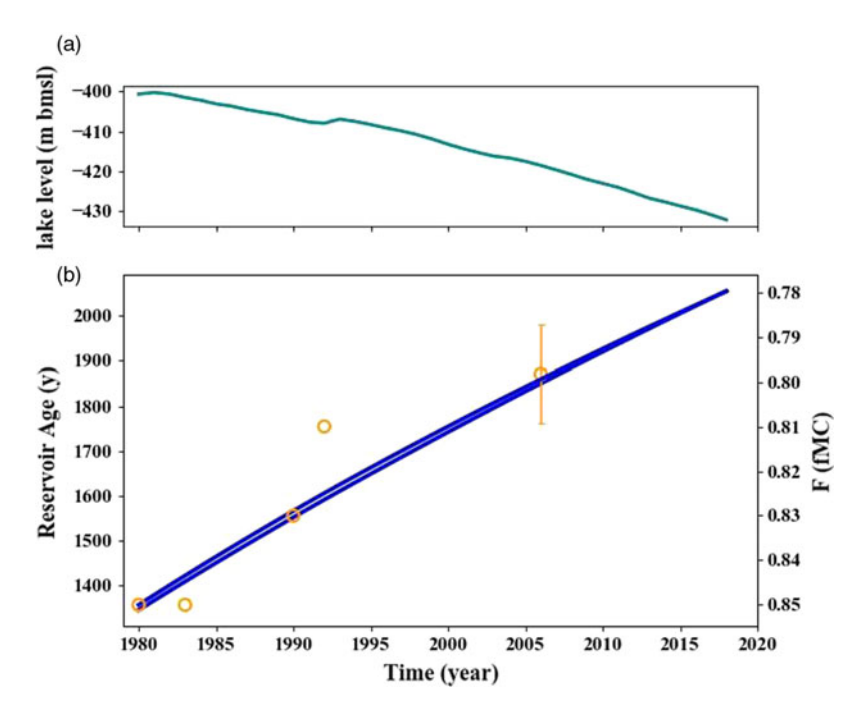


Figure 3 (a) Dead Sea level between the years 1980 and 2019, showing a decline from 400 to 432 m bmsl (Hydrological Service of Israel); (b) Reservoir age and <sup>14</sup>C fraction of the modern Dead Sea (F) during that time period (open circles) and model result as estimated from the DIC and <sup>14</sup>C mass-balance model (blue lines). Note that the right *y*-axis (F values) is reversed. The error bar for year 2006 represents an average of six values (data from Belmaker et al. 2007; Talma et al. 1997; Yechieli et al. 1996).

waters (fresh or saline) entering the lake; and (2) The climate conditions in the lake's watershed that dictate the amount of dissolved carbon in the influx source (e.g. the availability of calcite grains of dust origin that comprise the watershed surface cover, such as mountain soils, that are readily dissolved in the runoff water and make up the DIC of the influx).

The sensitivity of RA to environmental conditions was tested for two different scenarios of lake level change by running the mass balance model for carbon-radiocarbon as formulated by the equations in the section above. The first scenario was an attempt to reconstruct the RA during the last several decades of continuous lake level decline (Figure 3a) and low freshwater input as a result of anthropogenic manipulations. The radiocarbon content of the lake during this period was measured several times, allowing to calculate RA and testing the applicability of our mass-balance model (Figure 3b). The second scenario is a hypothetical case of rising lake level over a period of 100 yr at a rate of 10 cm·yr<sup>-1</sup>, resulting from an increase in Jordan River inflow (Figure 4). The input parameters used for calculating these two scenarios using the carbon-radiocarbon models are listed in Table 3. The changes in the volume and the surface area of the lake were calculated by the hypsometric curves of Hall (1997).

The modern lake level drop (Figure 3): During the last 50 years, the water level of the Dead Sea declined continuously (Figure 3a) as a result of anthropogenic intervention, mainly due to freshwater diversion and brine evaporation by potash industries. The recent level drop rate

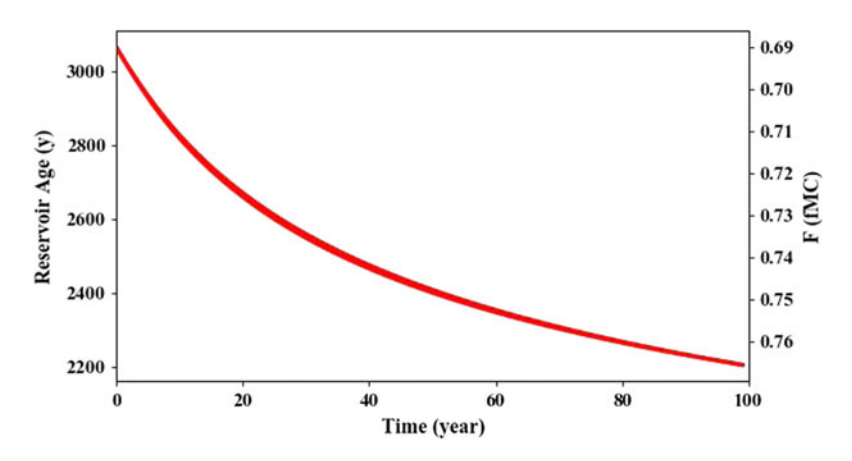


Figure 4 Reservoir age and the fraction of <sup>14</sup>C (F) in the lake in response to linear ascending lake level at a rate of 0.1 m·yr<sup>-1</sup> during 100 yr as calculated using the DIC and <sup>14</sup>C mass-balance model presented above. Note that the right *y*-axis (F) is reversed.

exceeds 1 m·yr<sup>-1</sup>, reaching 434.2 m bmsl in January 2020 (Israel Water Authority). In 1979 the water column of the Dead Sea overturned, ending a period of about 300 years of lake's stratification (Steinhorn et al. 1979; Stiller and Chung, 1984). Before the overturn, the epilimnion was characterized by higher radiocarbon content than the hypolimnion (0.78 fMC and 0.72 fMC, respectively, Neev and Emery, 1967). After the overturn, the lake was characterized by high radiocarbon of 0.85 fMC (Talma et al. 1997). This increase in the Dead Sea 14C might be due to the time gap between the sampling before and after the overturn and expresses mainly the effect of "bomb" 14C, entering the Dead Sea via freshwater runoff between 1960 to 1976 before the overturn (Talma et al. 1997). In the model, we used the documented data for the time interval 1980 to present, the time after the 1979 lake's overturn. We assume that during this period, several geochemicallimnologic parameters remained unchanged: runoff flow rate, partial pressure of dissolved CO<sub>2</sub> in the lake, CaCO<sub>3</sub> calcification rate, the operative piston velocity and the Henry constant. The model shows that during this period, the reservoir age of the Dead Sea increases monotonously by 700 yr, from 1350 yr to 2050 yr, and <sup>14</sup>C content dropped from 0.85 fMC (the value of 1980, after the overturn, Talma et al. 1997) to 0.78 fMC (Figure 3b). These trends fit rather well the documented <sup>14</sup>C data for the lake (Figure 3b), demonstrating the feasibility of this simple model for reconstructions of the <sup>14</sup>C content of the lake.

Hypothetical case of ascending lake level (Figure 4): This scenario assumes linearly ascending lake level at a rate of 0.1 m·yr<sup>-1</sup> during 100 yr (e.g., from 400 to 390 m bmsl), e.g. due to increased inflow of the Jordan River. The Jordan River flow corresponding to this ascending level rate was estimated from modeled relationship between the total yearly freshwater inflow to the Dead Sea, the annual precipitation rate and the corresponding lake level change (using the model of Morin et al. 2018). Here we arbitrarily started with RA of 3000 yr (a reasonable value estimated for historical lake level rise, Stein et al. 2004) and calculated the change in RA over 100 yr (Figure 4). In the calculation, we assumed that the partial pressure of dissolved CO<sub>2</sub> in the lake and CaCO<sub>3</sub> precipitation rate were dependent on the amount of DIC in the lake; and that during that period, thermodynamic constants

Table 3 Carbon, radiocarbon and water flow parameters (reported values presented up to 3 significant digits) used in the mass balance model\*.

Variable	Value	Units	Source
$\overline{\mathrm{Q}_{\mathrm{fl}}}$	$10 \cdot 10^{6}$	$m^3 \cdot yr^{-1}$	Lensky et al. (2005)
$Q_{sp}$	$210 \cdot 10^{6}$	$m^3 \cdot yr^{-1}$	Lensky et al. (2005)
$Q_{ss}^{T}$	$10 \cdot 10^{6}$	$m^3 \cdot yr^{-1}$	Weber et al. (2018)
$Q_{Jo}$	$105 \cdot 10^{6}$	$m^3 \cdot yr^{-1}$	Lensky et al. (2005)
$DIC_{fl}$	1.5	$\text{mol}\cdot\text{m}^{-3}$	Belmaker et al. (2007)
$DIC_{sp}$	4.6	$\text{mol}\cdot\text{m}^{-3}$	Avrahamov et al. (2010)
$DIC_{ss}$	3.3	$\text{mol} \cdot \text{m}^{-3}$	
$DIC_{Jo}$	1.1	$\text{mol}\cdot\text{m}^{-3}$	
$R_{CaCO_3}$	1.1	$\text{mol} \cdot \text{m}^{-2} \cdot \text{yr}^{-1}$	Golan et al. (2017)
$k_{PV_{DS}}$	4.5	$m \cdot yr^{-1}$	Golan et al. (2017)
$k'_{H_{DS}}$	2.98	$\text{mol} \cdot \text{m}^{-3} \cdot \text{atm}^{-1}$	Golan et al. (2016)
$P_{CO_{2DS}}$	1770	μatm	Golan et al. (2017)
$F_{fl}$	0.885	fMC	Talma et al. (1997); Belmaker et al. (2007)
$F_{sp}$	0.497	fMC	Yechieli et al. (1996); Avrahamov et al. (2010)
$F_{ss}$	0.075	fMC	Weber et al. (2018)
$F_{jo}$	0.84	fMC	Talma et al. (1997); Belmaker et al. (2007)
F <sub>atm</sub>	1	fMC	Reimer et al. (2013)

<sup>\*</sup>The absolute values in this table are approximations for the purpose of running the model. These values are based on estimates from the quoted studies, some of which show ranges of values, which were not taken into account here.

did not vary. The simulation of the mass-balance model shows that the response to lake level rise is a decrease in RA by ~1000 yr and an increase in F by 0.08 fMC (Figure 4).

### Radiocarbon Reservoir Age (RA) and the Age of Primary Aragonite

A plot of radiocarbon ages of the primary aragonites from the late Holocene section as a function of the radiocarbon ages of organic debris from the same stratigraphic unit shows a very good linear correlation (R<sup>2</sup>=0.98, Figure 5a). The linear correlation suggests that during that period, lake's RA remained rather stable (the intercept of the linear fit in Figure 5a), since large variations in RA would produce large deviations from a linear behavior. The stable RA in turn, is consistent with stable hydro-climate conditions in the lake watershed, namely that the supply of freshwater and brines was quite uniform. The good linear correlation between the radiocarbon ages of aragonites and organic debris provides a way to correct the apparent aragonite ages in section of the late Holocene Ze'elim Fm. where organic debris are not found (see below).

Another noteworthy observation is that the correlation line between the apparent aragonite ages ( $t_{app}$  in Figure 5a) and the organic debris "real" ages ( $t_{real}$  in Figure 5a) is higher by ~8% than unity (slope of 1.08, Figure 5a). The meaning of this small but distinct deviation from a unity slope is explained in the following paragraphs.

Three different ages were discussed above: (1)  $t_{real}$  - "real"  $^{14}C$  age of the organic debris as measured by AMS from the same horizon as the aragonite; (2)  $t_{RA}$  - the reservoir age (RA) at the time of aragonite precipitation; and (3)  $t_{app}$  - "apparent"  $^{14}C$  age of the aragonite as calculated from its measured  $^{14}C$  content.

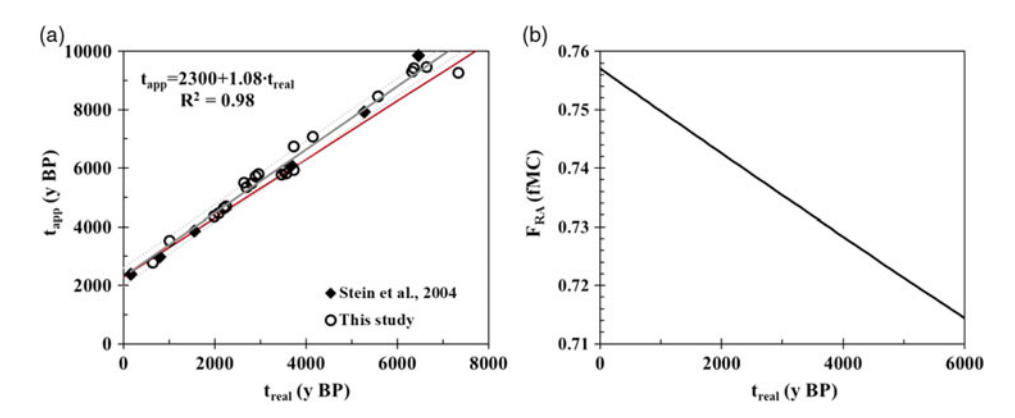


Figure 5 (a)  $t_{app}$  (the  $^{14}$ C age of aragonite sediments) versus  $t_{real}$  ( $^{14}$ C age of organic matter from the same sample) at various locations in Holocene sections from the Dead Sea shore (data from Table 1). The gray line is the linear regression of the data (Eq. 8), the dashed lines are the borders of mean squared error of the points in relation to the regression line ( $\pm 300$  yr) and the red line is a linear line with slope 1 with the same intercept as in Eq. (8) (2300 yr); (b) plot of Eq. (11) showing that for the time interval of 6000 yr, the exponential decrease of  $F_{RA}$  with time is in fact undistinguished from linear (see text).

If for the time interval under discussion (the last 6 kyr) the reservoir age  $(t_{RA})$  is constant, then the apparent age  $(t_{app})$  as a function of the "real" age  $(t_{real})$  should define a linear trend with slope  $a_1 = 1$  and intercept  $a_0 = t_{RA}$ :

$$t_{app} = t_{RA} + t_{real} \tag{7}$$

However, the best fit for the  $t_{app}$  vs.  $t_{real}$  line during the last 6 kyr (Figure 5a) is actually:

$$t_{app} = 2300 + 1.08 \cdot t_{real}$$
 (8)

This means that in Eq. (8),  $a_0 = t_{RA} = 2300$  yr and  $a_1 = 1.08$ , suggesting that  $t_{RA}$  (and hence also  $F_{RA}$  as defined in Eq. 1) is not constant, but rather increases linearly with time, during the last 6 ky, as shown by rewriting Eq. (8) to the form:

$$t_{app} = t_{RA,0} + 0.08 \cdot t_{real} + t_{real} \tag{9}$$

 $t_{\rm RA,0}$  in Eq. (9) is  $t_{\rm RA}$ =2300 yr (Eq. 8), which represents the average present-day reservoir age (at time zero). The reservoir age increases linearly with age (with a slope of 1.08–1=0.08) according to the equation:

$$t_{RA} = t_{RA,0} + 0.08 \cdot t_{real} \tag{10}$$

This implies that the reservoir age,  $t_{RA}$ , decreased with time: it was ~2780 yr at 6 ka and is ~2300 yr at present.

Substituting Eq. (10) into the exponential form of Eq. 1 yields:

$$F_{RA} = F_{atm} \cdot e^{-\lambda \cdot (t_{RA,0} + 0.08 \cdot t_{real})}$$

$$\tag{11}$$

Eq. (11) shows that the F of the Dead Sea ( $F_{RA}$ ) increased exponentially (with respect to the F of the present atmosphere) over the past ~6 kyr. However, in reality, at that time period,  $F_{RA}$ 

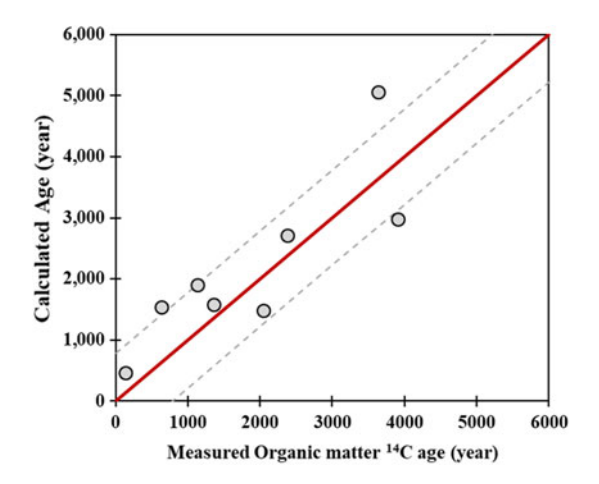


Figure 6 <sup>14</sup>C ages of CaCO<sub>3</sub> trapped in gypsum as calculated by Eq. (8) (Figure 5a) versus <sup>14</sup>C ages of organic debris (atmospheric ages) from same stratigraphic horizons. The red line has a slope of 1 and intercept of 0. Both ages agree within ±780 yr (the area between the two dashed lines, see text).

behaves nearly linearly with time (Figure 5b). Indeed, an expansion of Eq. (11) shows a linear behavior of the form (see details in Appendix 1):

$$F_{RA} = e^{-\lambda \cdot t_{RA,0}} - e^{-\lambda \cdot t_{RA,0}} \cdot \lambda \cdot 0.08 \cdot t_{real}$$
(12)

Eq. (12) shows that  $F_{RA}$  is a linear function of time with intercept of:  $F_{RA,0} = e^{-\lambda \cdot t_{RA,0}}$  and a slope of:  $-e^{-\lambda \cdot t_{RA,0}} \cdot \lambda \cdot 0.08$ . The linear Eq. (12) reproduces extremely well the  $F_{RA}$  values obtained from Eq. (8) up to  $t_{real} = 3000$  yr and yields a slightly lower  $F_{RA}$  value at  $t_{real} = 6000$  yr. The small linear increase in  $F_{RA}$  (the slope of Eq. 12) over the last 6 kyr is further elaborated in the next section, which discusses the secular trend in reservoir ages of the Holocene Dead Sea and its hydro-geological meaning.

The good linear correlation between  $t_{app}$  and  $t_{real}$  (Figure 5a) provides a possibility to apply Eq. (8) for calculating "real" ages of various authigenic (evaporite) deposits on the shores of the mid Holocene Dead Sea that are deficient of organic debris. The applicability of this dating method is demonstrated by the rather good correlation with an uncertainty of  $\sim \pm 800$  yr between  $^{14}C$  ages of aragonite "embedded" within the bulk gypsum that were calculated by Eq. (8) and the  $^{14}C$  ages determined on organic debris from the same stratigraphic units (Figure 6). The section below discusses the hydro-geological meaning of lake's  $F_{RA}$  trend during the last several thousand years.

#### Reservoir Ages and Hydro-Geological Settings of the Holocene Dead Sea

RA in the last glacial (MIS2) Lake Lisan was relatively low and its F approached the atmospheric value (Schramm et al. 2000; van der Borg et al. 2004). This reflects the enhanced bicarbonate load of freshwater (the product DIC<sub>total input</sub>·Q<sub>total input</sub> which is the sum of all inputs into the lake, in the mass-balance model described by Eq. 2) that equilibrated with atmospheric CO<sub>2</sub> (Schramm et al. 2000; Belmaker et al. 2007; Stein et al. 2013). The high bicarbonate load in

the brine during the Lisan period resulted from both, high freshwater runoff and high dust flux to the watershed that supplied fine calcite grains for dissolution (elaborated below). The transition from the late Lake Lisan to the Holocene Dead Sea was characterized by significant lake level drop, from ~200 to ~400 m bmsl, reflecting more arid conditions in the watershed and hence, reduced supply of freshwaters to the lake (e.g. Stein 2001; Migowski et al. 2006). The changes in the hydrologic conditions in the lake's watershed was accompanied by changes in the sedimentary facies that comprise the sedimentary sequences. While the typically high stand Lake Lisan was characterized by sedimentation of annual couplets of primary aragonite and silty detritus (e.g. the so-called aad facies, Machlus et al. 2000), the Holocene Dead Sea precipitated mainly sequences of silty detritus or "muds" (the ld facies, Haliva-Cohen et al. 2012). Nevertheless, the past 3000 yr in the history of the Dead Sea were characterized by deposition of sequences of the aad couplets or detritus, aragonite and gypsum triplets, both marking a resumed supply of freshwaters loaded with bicarbonate and sulfate to the lake (Migowski et al. 2006; Kagan et al. 2015; Belmaker et al. 2019).

At the early Holocene (from  $\sim$ 10 to  $\sim$ 6.2 cal kyr BP) the RA (and  $F_{RA}$ ) fluctuated between 1940 and 7590 (Figures 7a, b), while the atmospheric <sup>14</sup>C values at that time remained almost constant (Figure 7b, IntCal13, Reimer et al. 2013). A maximum RA of 6 kyr (minimum F<sub>RA</sub>) (Figures 7a, b), is recorded at ~8 cal kyr BP, when the lake receded to a minimum level of less than 420 m bmsl (Figure 7c). This extremely high RA (and low F<sub>RA</sub>) was explained by an enhanced contribution of saline waters with very low fMC (Stein et al. 2004). The outflow of saline springs waters may have been larger just after the major lake level decline than their present flow (e.g., the Ein Qedem saline hydrothermal spring system, Weber et al. 2018).

This rather "noisy" behavior of  $F_{RA}$  (and RA) was replaced by a good linear  $F_{RA}$  increase and RA decrease starting at ~ 6 cal kyr BP (Figures 5 and 7a, b). During the Mid-Holocene period (~6–3.6 cal kyr BP), Dead Sea levels were relatively high (Figure 7c), reaching ~380 m bmsl, with several large and fast fluctuations (Migowski et al. 2006). These fluctuations in lake level are reflected as deviations from the linear trends in the RA and F<sub>RA</sub> (the red lines in Figures 7a, b). For example, during the sharp rise in lake level at ~4–3.6 cal kyr BP (Figure 7c), when the lake rose from  $\sim$ 400 to  $\sim$ 380 m bmsl,  $F_{RA}$  plots above the trend line (which represents the longterm F<sub>RA</sub> increase in the lake, see discussion below), while the RA plots below the trend line. We suggest that enhanced inflow of freshwater (e.g. Jordan River and runoff from Judea Mountains), represented by the sharply ascending lake level, contributed high radiocarbon DIC to the lake, similar to the scenario shown in Figure 4.

During the past 3 ky, lake level was relatively low and showed a slow long-term level increase (by  $\sim 15$  m) with several fluctuations (Figure 7c). The best linear fit for the plot of RA vs.  $t_{real}$ during this period (Figure 7a, black line) has a higher slope than the slope of the trend line for the entire past 6 kyr period (Figure 7a, red line). This suggests that the effect of lake level change on the F<sub>RA</sub> of the Dead Sea during the last 3 kyr was larger than its overall (average) effect during the last 6 kyr. A plot of the difference between F<sub>RA</sub> and F<sub>atm,t</sub> (orange triangles in Figure 7b), as a proxy for RA, shows that it decreased due to the change in the radiocarbon content of the lake and not due to variation in atmospheric radiocarbon.

We suggest that the long-term RA decrease during the past 3 kyr period reflects an enhanced supply of bicarbonate ions by freshwater runoff where radiocarbon equilibrated with the atmosphere. The enhanced bicarbonate load occurred during periods of lake's low stands,

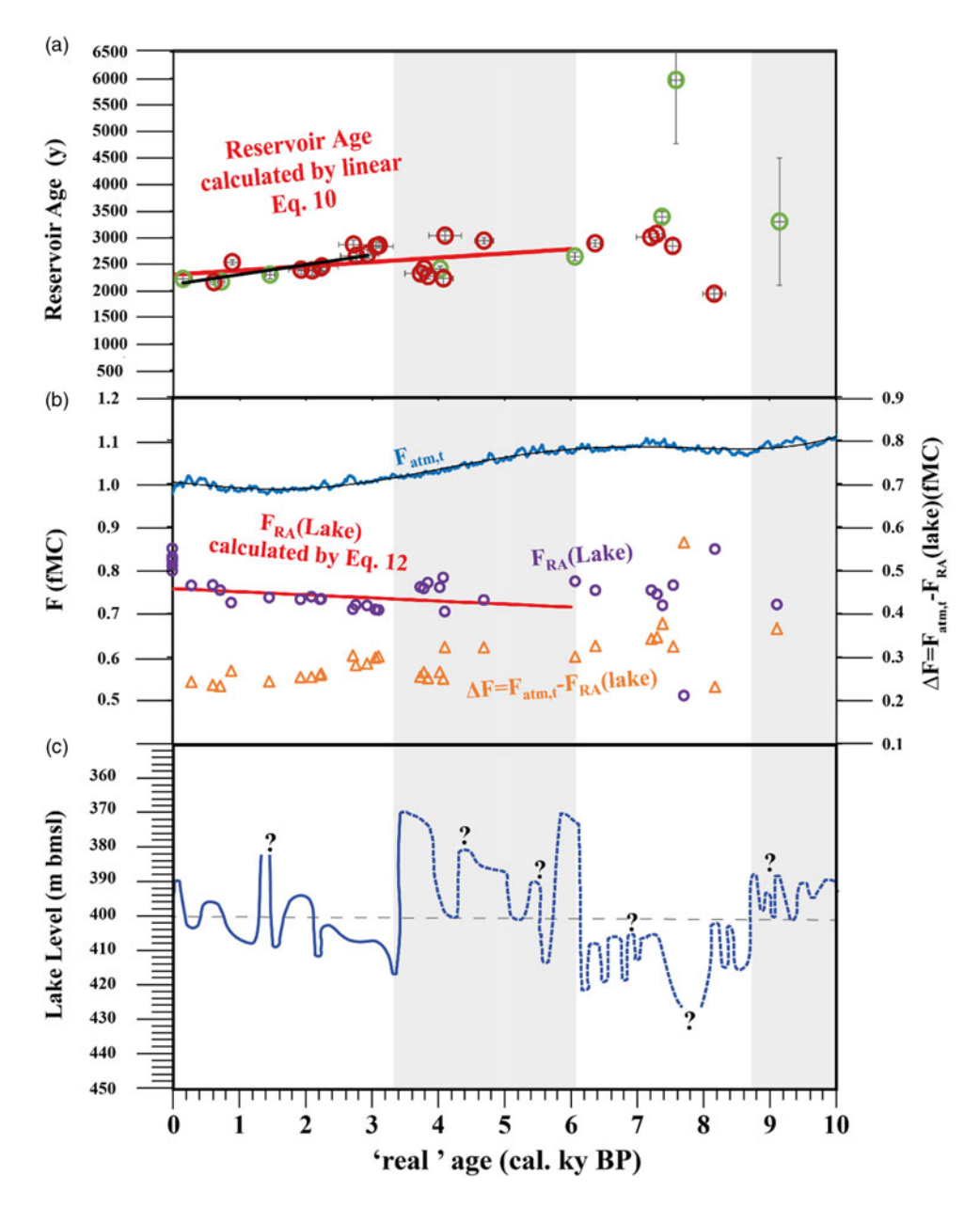


Figure 7 Secular variations of radiocarbon related parameters in the Holocene Dead Sea. (a) Measured RA (red circles data from this study and green circles data from Stein et al. 2004), the crosses represent the propagated error calculated from  $^{14}\mathrm{C}$  uncertainties on organic matter and aragonite (see footnote of Table 1), RA calculated by Eq. (10) for the last 6000 yr (red line) and the linear relation in the past 3000 yr (black line); (b)  $F_{atm,t}$  represents the IntCal13 of the Northern Hemisphere recalculated in fMC units (blue line, data from Reimer et al. 2013), the  $F_{RA}$  of the lake at the time that the aragonite precipitated (purple circles) calculated from the difference between aragonite radiocarbon and the radiocarbon of organic material from the same stratigraphic horizon, the  $F_{RA}$  calculated by Eq. (12) (red line) and  $\Delta F$ , which is the difference between IntCal13 curve ( $F_{atm,t}$ ) and  $F_{RA}$  of the lake (orange triangles, secondary *y*-axis); (c) Fluctuations in lake level during the last 10 kyr (after Migowski et al. 2006). The two gray shaded areas mark periods of lake level  $\geq$  400 m bmsl.

stems probably from the high input of dust to the region at the end of the African wet period (Belmaker et al. 2014, 2019; Kagan et al. 2015; Stein 2014). Enhanced dust input increased the DIC (as well as calcium) in the runoff due to preferential dissolution of the fine calcite grains that make up ~30–40% of the dust transported to the regional drainage area (Belmaker et al. 2007; Palchan et al. 2018b). The Sr isotopic composition of lake's brine (both the Holocene Dead Sea and Lake Lisan) and present-day runoff support this suggestion. The <sup>87</sup>Sr/<sup>86</sup>Sr ratios of the lake's brine and runoff is ~0.7080, similar to that of the detrital calcites comprising the desert dust, but differ significantly from the 87Sr/86Sr ratios of the Cretaceous carbonates (limestone and dolomite) exposed in the watershed (Palchan et al. 2018a). It is likely that the availability of easily dissolved fine calcite particles, increased the bicarbonate load of the runoff (the product DICtotal input Qtotal input, see above) by increasing its DIC, despite the rather low, but steadily increasing, flow rate (Q), which is reflected in the rise of the lake level (see Figure 7c and discussion above). In contrast to the observed long-term decrease in RA as discussed above (Figure 7a), during the last ~40 yr the Dead Sea shows a substantial RA increase by ~700 yr and  $F_{RA}$  decrease by ~0.07 (Figure 3b). The long-term trends reversed as a result of the sharp decline in lake level (not shown in Figure 7c, but the last 38 y are shown in Figure 3a) caused by modern anthropogenic perturbations, mainly freshwater diversion and evaporite minerals production.

The RA values of the last glacial Lake Lisan show a continuous decrease during its high stand period (~30–17.4 cal kyr BP), when the lake deposited sequences of primary aragonite and silty detritus that mark supply of dissolved bicarbonate ions to the lakes (Stein et al. 2013). Both last glacial and late Holocene periods were characterized by enhanced transport of desert dust from the north Sahara deserts to the southern Levant, forming the surface cover of the Dead Sea watershed (Haliva-Cohen et al. 2012). The dissolution of the detrital calcites comprising the surface cover appears to impact the radiocarbon budget of the lake.

### **SUMMARY**

The fraction of radiocarbon in the Dead Sea is dictated by two major sources, a "very young" DIC (dissolved inorganic carbon with high radiocarbon content) in runoff freshwater that interacted with atmospheric CO2 and "old" carbon supplied by underground brines (e.g., the saline springs of Ein Qedem). Secular variations in these radiocarbon sources during the last 6 kyr are recorded in the sedimentary sections of the Holocene Dead Sea (Ze'elim Fm.) as variations in lake's reservoir age (RA). The RA of the lake is defined as the difference between the radiocarbon age of the aragonite in the section (a primary authigenic mineral) at time of its precipitation (representing lakes' DIC) and the age of contemporaneous organic debris (representing atmospheric radiocarbon). Lake's RA is determined by the regional hydrological regime, hence, secular variations in RA can be used as regional paleo-hydrological proxies.

In this study, we report on new radiocarbon data of organic debris and primary authigenic aragonite sampled from exposures of the Holocene Ze'elim Fm. along the retreating shores of the modern Dead Sea. We used these new data together with earlier radiocarbon data to reconstruct the history of radiocarbon in the Holocene Dead Sea and discuss the hydrogeological processes controlling its RA. The Holocene data are considered in light of radiocarbon content of the modern lake and are compared with previous radiocarbon data on both the Holocene Dead Sea and the last glacial Lake Lisan.

A simple mass-balance box model for DIC and radiocarbon was constructed to evaluate the effect of various inputs and outputs and lake's level changes on the RA of the modern Dead Sea. The model shows that during the sharp anthropogenic lake level drop of the past 40 yr, RA of the Dead Sea increased monotonously by ~700 yr, and its <sup>14</sup>C content decreased due to the steady shrinking in lake's size. The modern sharp decreasing trend of the lake level reversed the long-term trend of the 6 kyr of gradual RA decrease (with short occasional reversals).

During the past 6 kyr, radiocarbon ages of the aragonites of the Holocene section correlate linearly with the radiocarbon ages of organic debris from the same stratigraphic unit ( $R^2$ =0.98). This correlation can be used to estimate ages of primary (evaporite) deposits on the shores of the mid-Holocene Dead Sea where organic debris are not available.

The RA during this period was quite uniform and changed only by  $\sim$ 480  $\pm$  300 yr, decreasing from 2890 to 2300 yr. This uniformity in the RA reflects the overall stability of the hydrological-climate conditions in the Dead Sea watershed that dictated uniform input of dissolved bicarbonate to the lake. The RA of the Dead Sea during early Holocene showed larger fluctuations between  $\sim$ 6 and  $\sim$ 3 cal kyr BP. The highest RA values are recorded in early Holocene lake at 8.5-8.1 cal kyr BP, possibly reflecting the significant decrease in the freshwater input and lake level at that time and an enhanced contribution of saline waters with very low radiocarbon content (e.g. Ein Qedem type). It appears that just after the major lake level decline, the outflow of these saline springs was larger than their present flow.

The fluctuations in RA around the linear trend mean that the overall uniform hydro-climate conditions in the late Holocene Dead Sea watershed were punctuated by short episodes of enhanced/reduced freshwater supply to the lake that were reflected by abrupt lake rises and drops.

During the past 3 kyr, the RA show a small temporal decrease from 3100 to 2200. A similar decrease (~2000 yr) was reported for the last glacial MIS2 (~30–17.4 cal kyr BP) Lake Lisan. Both decreases are explained by continuous supply of bicarbonate from the lake by freshwater runoff that dissolved detrital calcites comprising the surface cover of the lakes' watershed.

### **ACKNOWLEDGMENTS**

The paper is dedicated to the late Prof. Wally Broecker, who pioneered the investigation of radiocarbon in the Dead Sea lacustrine system. We thank Tim Jull and team of the NSF-BSF radiocarbon facility at Arizona. We thank the staff of the National Ocean Sciences Accelerator Mass Spectrometry (NOSAMS) facility, Woods Hole Oceanographic Institution (WHOI), Woods Hole, MA, for providing the first author (NW) a working space, helping her in the submission of a successful travel grant and in the analytical process. We wish to thank the associate editor Quan Hua, the reviewer Mariana Stiller and an additional anonymous reviewer for their fruitful and insightful comments and suggestions that helped to improve the manuscript. We thank the BSF Rahamimoff Travel Grant for Young Scientists which funded the travel expenses of NW to NOSAMS. This work was supported by the Israeli government under GSI DS project 40573, the PALEX project "Paleohydrology and Extreme Floods from the Dead Sea ICDP Core", funded by the DFG, Germany (Grant No. BR2208/13-1/-2 to BL and MS) and the Dead Sea Excellence Center of the Israel Science Foundation (grant 1736/11 to BL).

#### REFERENCES

- Avrahamov N, Yechieli Y, Lazar B, Lewenberg O, Boaretto E, Sivan O. 2010. Characterization and dating of saline groundwater in the Dead Sea area. Radiocarbon 52(2):1123-1140.
- Bartov Y, Goldstein SL, Stein M, Enzel Y. 2003. Catastrophic arid episodes in the Eastern Mediterranean linked with the North Atlantic Heinrich events. Geology 31(5):439.
- Bartov Y, Stein M, Enzel Y, Agnon A, Reches Z. 2002. Lake Levels and Sequence Stratigraphy of Lake Lisan, the Late Pleistocene Precursor of the Dead Sea. Quaternary Research 57(1):9-21.
- Begin ZB, Broecker W, Buchbinder B, Druckman Y, Kaufman A, Magaritz M, Neev D. 1985. Dead Sea and Lake Lisan levels in the last 30,000 years. Israel Geological Survey Report 29/85:1-17.
- Belmaker R, Lazar B, Stein M, Taha N, Bookman R. 2019. Constraints on aragonite precipitation in the Dead Sea from geochemical measurements of flood plumes. Quaternary Science Reviews
- Belmaker R, Stein M, Beer J, Christl M, Fink D, Lazar B. 2014. Beryllium isotopes as tracers of Lake Lisan (last Glacial Dead Sea) hydrology and the Laschamp geomagnetic excursion. Earth and Planetary Science Letters 400:233-242.
- Belmaker R, Stein M, Yechieli Y, Lazar B. 2007. Controls on the radiocarbon reservoir ages in the modern Dead Sea drainage system and in the Last Glacial Lake Lisan. Radiocarbon 49(2):969-982.
- Bookman R, Enzel Y, Agnon A, Stein M. 2004. Late Holocene lake levels of the dead sea. Bulletin of the Geological Society of America 116(5-6): 555-571.
- Bookman R, Lazar B, Stein M, Burr GS. 2007. Radiocarbon dating of primary aragonite by sequential extraction of CO<sub>2</sub>. Holocene 17(1): 131-137.
- Golan R, Gavrieli I, Ganor J, Lazar B. 2016. Controls on the pH of hyper-saline lakes - A lesson from the Dead Sea. Earth and Planetary Science Letters 434:289-297.
- Golan R, Lazar B, Wurgaft E, Lensky N, Ganor J, Gavrieli I. 2017. Continuous CO2 escape from the hypersaline Dead Sea caused by aragonite precipitation. Geochimica et Cosmochimica Acta 207:43-56.
- Haase-Schramm A, Goldstein SL, Stein M. 2004. U-Th dating of Lake Lisan (late Pleistocene Dead Sea) aragonite and implications for glacial east Mediterranean climate change. Geochimica et Cosmochimica Acta 68(5): 985-1005.
- Haliva-Cohen A, Stein M, Goldstein SL, Sandler A, Starinsky A. 2012. Sources and transport routes of fine detritus material to the Late Quaternary Dead Sea basin. Quaternary Science Reviews 50:55-70.

- Hall JK. 1997. Topography and bathymetry of the Dead Sea depression. In: Niemi TM, Ben-Avraham Z, Gat JR, editors. The Dead Sea: The Lake and its setting. New York: Oxford University Press. p. 11–21.
- Kagan EJ, Langgut D, Boaretto E, Neumann FH, Stein M. 2015. Dead Sea levels during the Bronze and Iron Ages. Radiocarbon 57(2):237-252.
- Ken-Tor R, Agnon A, Enzel Y, Stein M, Marco S, Negendank JFW. 2001. High-resolution geological record of historic earthquakes in the Dead Sea basin. Journal of Geophysical Research: Solid Earth 106(B2):2221-2234.
- Lensky NG, Dvorkin Y, Lyakhovsky V, Gertman I, Gavrieli I. 2005. Water, salt, and energy balances of the Dead Sea. Water Resources Research 41(12):1–13.
- Machlus M, Enzel Y, Goldstein SL, Marco S, Stein M. 2000. Reconstructing low levels of Lake Lisan by correlating fan-delta and lacustrine deposits. Quaternary International 73:137-144.
- Migowski C, Stein M, Prasad S, Negendank JF, Agnon A. 2006. Holocene climate variability and cultural evolution in the Near East from the Dead Sea sedimentary record. Quaternary Research 66(3):421-431.
- Morin E, Ryb T, Gavrieli I, Enzel Y. 2018. Mean, variance, and trends of Levant precipitation over the past 4500 years from reconstructed Dead Sea levels and stochastic modeling. Quaternary Research 2018:1-17.
- Müller G, Gastner M. 1971. The "Karbonat-Bombe", a simple device for the determination of carbonate content in sediment, soils, and other materials, Neues Jahrbuch für Mineralogie - Monatshefte, Bremerhaven. PANGAEA 10:466-469.
- Neev D, Emery KO. 1967. The Dead Seadepositional processes and environments of evaporites. Jerusalem.
- Palchan D, Erel Y, Stein, M. 2018a. Geochemical characterization of contemporary fine detritus in the Dead Sea watershed. Chemical Geology 494(April):30-42.
- Palchan D, Stein M, Goldstein SL, Almogi-Labin A, Tirosh O, Erel Y. 2018b. Synoptic conditions of fine-particle transport to the last interglacial Red Sea-Dead Sea from Nd-Sr compositions of sediment cores. Quaternary Science Reviews 179:123-136.
- Prasad S, Negendank JFW, Stein M. 2009. Varve counting reveals high resolution radiocarbon reservoir age variations in palaeolake Lisan. Journal of Quaternary Science 24(7):690–696.
- Reimer PJ, Bard E, Bayliss A, Beck JW, Blackwell PG, Bronk Ramsey C, Buck C, Cheng H, Edwards RL, Friedrich M, et al. 2013. IntCal13 and Marine13 radiocarbon age calibration curves 0-50,000 years cal BP. Radiocarbon 55(4): 1869-1887.

- Roberts ML, Beaupré SR, Burton JR. 2013. A highthroughput, low-cost method for analysis of carbonate samples for <sup>14</sup>C. Radiocarbon 55(2): 585-592.
- Schramm A, Stein M, Goldstein SL. 2000. Calibration of the <sup>14</sup>C time scale to >40 ka by <sup>234</sup>U-<sup>230</sup>Th dating of Lake Lisan sediments (last glacial Dead Sea). Earth and Planetary Science Letters 175(1-2):27-40.
- Stein M. 2001. The sedimentary and geochemical record of neogene-quaternary water bodies in the Dead Sea basin-inferences for the regional paleoclimatic history. Journal of Paleolimnology 26:271-282.
- Stein M. 2014. The evolution of Neogene-Quaternary water-bodies in the Dead Sea Rift Valley. Dordrecht: Springer. p. 279-316.
- Stein M, Agnon A, Katz A, Starinsky A. 2002. Strontium isotopes in discordant dolomite bodies of the Judea Group, Dead Sea basin. Israel Journal of Earth Sciences, 51(3-4), 219-224.
- Stein M, Goldstein LS, Schramm A. 2000. Radiocarbon calibration beyond the dendrochronology range. Radiocarbon 42(3):415-422.
- Stein M, Lazar B, Goldstein SL. 2013. Radiocarbon reservoir ages as freshwater-brine monitors in Lake Lisan, Dead Sea system. Radiocarbon 55:1050-1057.
- Stein M, Migowski C, Bookman R, Lazar B. 2004. Temporal changes in radiocarbon reservoir age in the Dead Sea-Lake Lisan system. Radiocarbon 46:649-655.
- Steinhorn I, Assaf G, Gat JR, Nishry A, Nissenbaum A, Stiller M, Beyth M, Neev D, Garber R,

- Friedman GM, et al. 1979. The Dead Sea: Deepening of the mixolimnion signifies the overture to overturn of the water column. Science 206(4414):55-57.
- Stiller M, Chung YC. 1984. Radium in the Dead Sea: A possible tracer for the duration of meromixis 1. Limnology and Oceanography 29(3):574-586.
- Stuiver M, Polach HA. 1977. Discussion: Reporting of <sup>14</sup>C data. Radiocarbon 19(3): 355-363.
- Talma AS, Vogel JC, Stiller M. 1997. The radiocarbon content of the Dead Sea. In: Niemi TM, Ben-Avraham Z, Gat Y, editors. The Dead Sea-the lake and its setting. Oxford: Oxford University Press. p. 171-183.
- Torfstein A, Goldstein SL, Stein M, Enzel Y. 2013. Impacts of abrupt climate changes in the Levant from Last Glacial Dead Sea levels. Quaternary Science Reviews 69:1-7.
- van der Borg K, Stein M, de Jong AFM, Waldmann ND, Goldstein SL. 2004. Near-zero  $\Delta^{14}$ C values at 32 kyr cal BP observed in the high-resolution <sup>14</sup>C record from U-Th dated sediment of Lake Lisan. Radiocarbon 46(2):785–795.
- Weber N, Yechieli Y, Stein M, Gavrieli I, Yokochi R, Zappala J, Mueller P, Lazar B. 2018. The circulation of the Dead Sea brine in the regional aquifer. Earth and Planetary Science Letters 493:242-261.
- Yechieli Y, Ronen D, Kaufman A. 1996. The source and age of ground water brines in the Dead Sea area, as deduced from 36Cl and 14C. Geochimica et Cosmochimica Acta 60(11): 1909-1916.

#### APPENDIX 1

## Linear Expansion of Eq. (11)

Eq. (11),  $F_{RA} = F_{atm} \cdot e^{-\lambda \cdot \left(t_{RA,0} + 0.08 \cdot t_{real}\right)}$ , is in fact a linear equation because the value of  $\lambda \cdot 0.08 \cdot t_{real}$ , the second term in the exponent of Eq. (11), is very close to zero for  $t_{real}$  of several thousand years (the time interval discussed here). Rewriting Eq. (11) yields:

$$F_{RA} = F_{atm,t} \cdot e^{-\lambda \cdot t_{RA,0}} \cdot e^{-\lambda \cdot 0.08 \cdot t_{real}} \tag{i}$$

Expansion of the right-hand term in Eq. (i),  $f(t) = e^{-\lambda \cdot 0.08 \cdot t_{real}}$ , by Maclaurin infinite series of a function  $f(x) = \sum_{n=0}^{n=\infty} \frac{f(0)^{(n)}}{n!} \cdot x^n$  around the value x=0, which for the function  $f(x) = e^x$ (where  $x = -\lambda \cdot 0.08 \cdot t_{real}$ ) yields:

$$e^{x} = 1 + x + \frac{1}{2} \cdot x^{2} + \cdots$$
 (ii)

Substituting just the linear part of Eq. (ii)  $(e^x = 1 + x)$  into Eq. (i) yields a linear function of time:

$$F_{RA} = F_{atm,t} \cdot e^{-\lambda \cdot t_{RA,0}} \cdot (1 - \lambda \cdot 0.08 \cdot t_{real}) \tag{iii}$$

Defining  $F_{atm}=1$  (for present day) Eq. (iii) becomes Eq. (12):

$$F_{RA} = e^{-\lambda \cdot t_{RA,0}} - e^{-\lambda \cdot t_{RA,0}} \cdot \lambda \cdot 0.08 \cdot t_{real}$$